Journal of Catalysis **208,** 321–331 (2002)
doi:10.1006/jcat.2002.3604

Synthesis, Characterization, and Hydrotreating Activity of Several Iron Group Transition Metal Phosphides

Xianqin Wang, Paul Clark,[1] and S. Ted Oyama[2]

Environmental Catalysis and Materials Laboratory, Department of Chemical Engineering (0211), Virginia Polytechnic Institute and State University, Blacksburg, Virginia 24061

Received September 20, 2001; revised March 9, 2002; accepted March 9, 2002

A series of iron, cobalt, and nickel metal phosphides of chemical formula Fe_2P, CoP, and Ni_2P with specific surface areas of around 3 $m^2\,g^{-1}$ were synthesized by means of temperature-programmed reduction (TPR) of the corresponding phosphates. These phosphides were also successfully prepared in dispersed form on a silica support (90 $m^2\,g^{-1}$) for use as catalysts. The phase purity of these materials was established by X-ray diffraction (XRD), and surface properties were determined by N_2 BET specific surface area (S_g) measurements and CO uptake determinations. The activity of the silica-supported catalysts in hydrodenitrogenation (HDN) and hydrodesulfurization (HDS) was evaluated in a three-phase trickle-bed reactor using a model liquid feed containing 2000 ppm nitrogen as quinoline, 3000 ppm sulfur as dibenzothiophene, 500 ppm oxygen as benzofuran, 20 wt% aromatics as tetralin, and balance aliphatics as tetradecane. The reactivity study showed that the HDS activity sequence for the three samples was $Ni_2P/SiO_2 > CoP/SiO_2 > Fe_2P/SiO_2$, while the HDN activity followed the sequence $CoP/SiO_2 > Ni_2P/SiO_2 > Fe_2P/SiO_2$. Compared with a commercial Ni–Mo–S/γ-Al_2O_3 catalyst, Ni_2P/SiO_2 had a higher HDS activity (90 vs 76%), but a lower HDN activity (14 vs 38%), based on equal sites loaded in the reactor. The sites were determined by CO chemisorption for the phosphide and low-temperature O_2 chemisorption for the sulfide. XRD and X-ray photoelectron spectroscopy characterizations of the spent catalysts indicated that the Ni_2P/SiO_2 catalyst was tolerant of sulfur.

Key Words: **hydrodesulfurization; hydrodenitrogenation; transition metal phosphides; Fe_2P; CoP; Ni_2P.**

INTRODUCTION

Demands for a cleaner environment have led to a global tightening in the allowed sulfur content in fuels and increased restrictions on the release of nitrogen oxides. For example, in the case of sulfur the U.S. Environmental Protection Agency (EPA) has issued regulations that would lower its allowed content in diesel fuel from the current 500 to 15 ppmw in 2006, and in gasoline from 300 to 30 ppmw by 2004 (1, 2). For this reason there are considerable efforts being expended to develop new technologies for the production of clean fuels, like adsorption, extraction, oxidation, alkylation, and bioprocessing (3). Currently, however, hydroprocessing appears to be the technologically prefered solution (3). Hydroprocessing refers to a variety of catalytic hydrogenation processes that saturate heteroatomatic rings and remove S, N, O, and metals from different petroleum streams in a refinery (4). Because of the tighter environmental regulations new types of catalysts, which are economic, have long life, and possess high activity, are highly desired. In this work we present results on a new type of hydroprocessing catalyst: transition metal phosphides.

Transition metal phosphides have attracted considerable interest for some time because these materials are technologically important as semiconductors, luminescent devices, and electronic components (5). A brief thermodynamic analysis of the potential stability in H_2S was carried out early in 1975 (6), and it was revealed that this group of materials is potentially stable and sulfur resistant. However, the transition metal phosphides as a class of materials have received little attention in the field of catalysis. This is probably because the development of synthetic methods of producing materials with high surface areas was not achieved.

The combination of the iron group metals Co and Ni with Mo and W in commercial hydroprocessing catalysts (7–9) and the use of phosphorus as a promoter (10–12) is well-known. Many workers have studied the effect of phosphorus in sulfide catalysts (13–16), and the topic has been reviewed by Iwamoto and Grimblot (17). It was concluded that in these materials, the phosphorus was found as a phosphate and primarily modified the properties of the support, and only indirectly the active phase. For example, phosphorus altered the acid–base character of alumina and improved dispersion of molybdenum on the support. It also enhanced the solubility of the precursor metals in the preparation stages and allowed the synthesis of high-loading catalysts (18). The effect of phosphorus strongly depended on its content, with an effect that was usually negative at high

[1] Present address: Luna Innovations, 2851 Commerce St., Blacksburg, VA 24073.

[2] To whom correspondence should be addressed. E-mail: oyama@vt.edu.

0021-9517/02 $35.00

loadings. Phosphorus showed no effect or a small positive effect on the hydrodesulfurization (HDS) of thiophene, and a positive effect on the hydrodenitrogenation (HDN) of quinoline (19), pyridine (20), and piperidine (11). Notwithstanding the considerable studies on promoter effects, until recently phosphorus compounds in the form of phosphides had not been examined in the hydroprocessing field. The first report of the use of the iron group metal phosphides as hydrodenitrogenation catalysts was by Robinson *et al.* (21), who prepared Co_2P and Ni_2P on silica, alumina, and carbon. They reported that carbon and silica were the best supports and that Ni_2P, in particular, was very effective in HDN. These studies were carried out at high conversion, and an assessment of the intrinsic activity is not possible. The first studies on Mo and W phosphides were carried out by Li *et al*. (22), Oyama *et al.* (23), and Clark *et al.* (24), who reported good activity for HDS and HDN. Studies in the Prins group (25) confirmed the activity in HDN, and in a recent comparison of Co_2P, Ni_2P, MoP, CoMoP, and NiMoP (26) it was concluded that the areal activity of MoP was the highest. Earlier, the olefin hydrogenation activity of Ni_2P supported on alumina and other phosphides was explored by Nozaki and coworkers (27–29). It was found that the hydrogenation activity for butadiene drastically decreased, in the order $Ni_2P > Co_2P > FeP$. They also reported that a trace of oxygen could increase the activity of Ni_2P while lowering the activity of Ni for the butadiene hydrogenation reaction. Nickel–phosphorus alloys have been reported also in amorphous form and their activities for hydrogenation have also been studied (30, 31). The amorphous alloy was prepared by an electroless plating technique from mixtures of sodium citrate, nickel sulfate, sodium hypophosphite, sodium acetate, and a silica gel support, or by the chemical reduction of nickel acetate and sodium phosphate with sodium borohydride. The supported material was subjected to various treatments, including oxidation at 403 K and reduction in H_2 at 553 K. The catalyst was found to be active for the hydrogenation of nitrobenzene (32) and benzaldehyde (33), with a turnover rate similar to that of Ni (1×10^{-3} s^{-1}). In summary, although there are some reports concerning the catalytic behavior of these phosphides, few studies have concentrated on the subject of hydrodesulfurization and hydrodenitrogenation for application in petroleum refining.

The present work presents an in-depth study of the preparation of transition metal phosphides of the iron group (Fe, Co, Ni) and their evaluation in the hydroprocessing of a model feed mixture. Initially unsupported bulk materials were prepared to provide a reference for the synthesis of supported materials. Several metal-to-phosphorus (M/P) ratios were explored to ascertain which stable phases could be prepared and to determine the conditions for temperature-programmed reduction. Subsequently, the preparation was extended to the supported system to obtain materials of high surface area suitable for catalytic testing. Silica was chosen as the carrier to minimize support effects and make possible the elucidation of the intrinsic catalytic activity of the phosphides.

EXPERIMENTAL

Materials

The support used in this study was a fumed silica (Cabosil, L90). The precursors for iron, cobalt, and nickel were $Fe(NO_3)_3 \cdot 9H_2O$ (Aldrich, 99.99%), $Co(NO_3)_2 \cdot 6H_2O$ (Aldrich, 99.99%), and $Ni(NO_3)_2 \cdot 6H_2O$ (Aesar, 99%), respectively, while the precursor for P was ammonium orthophosphate $(NH_4)_2HPO_4$ (Aldrich, 99%). The chemicals utilized in the reactivity study were dibenzothiophene (Aldrich, 99.5%), quinoline (Aldrich, 99.9%), benzofuran (Aldrich, 99.9%), tetralin (Aldrich, 99.5%), and tetradecane (Jansen Chimica, 99%). The gases employed were He (Airco, Grade 5), CO (Linde Research Grade, 99.97%), 0.5% O_2/He (Airco, UHP Grade), H_2 (Airco, Grade 5), N_2 (Airco, 99.99%), and 30% N_2/He (Airco, UHP Grade).

Synthesis

Unsupported bulk transition metal phosphides were prepared in two steps. In the first step, phosphate precursors were synthesized by reacting metal nitrates with ammonium phosphate, and in the second step, these phosphates were reduced to phosphides by the method of temperature-programmed reduction. Because the procedures for preparing unsupported bulk iron, cobalt, and nickel phosphates were similar, the preparation of iron phosphate ($FePO_4$) is used here to illustrate the process. First, 4.9 g (37.13 mmol) of ammonium phosphate $(NH_4)_2HPO_4$ was dissolved in 300 cm^3 of distilled water to form a transparent colorless solution, and 15 g (37.13 mmol) of iron nitrate ($Fe(NO_3)_3 \cdot 9H_2O$) was then added. The clear solution immediately turned into a light color mixture with some precipitate, but stirring resulted in the formation of a transparent solution. In the case of nickel and cobalt, several drops of nitric acid were needed to give rise to a homogenous solution. The water was then vaporized from the solution on a hot plate and the resulting paste was dried at 393 K for 3 h and calcined at 773 K for 6 h in an oven. The amount collected (with some minor losses) was 5.54 g, which corresponds to 36 mmol of iron phosphate of formula $FePO_4 \cdot H_2O$. The phosphate was then ground with a mortar and pestle and sieved to 16/20 mesh (0.65- to 1.2-mm-diameter particles). In the second step of preparation, temperature-programmed reduction (TPR) was utilized to convert the phosphate into phosphide. The reduction was carried out in a U-shaped quartz reactor placed in a furnace controlled by a temperature programmer (Omega Model CN 2000). The temperature was raised at $\beta = 0.0167$ K s^{-1} (1 K min^{-1}) and was monitored by a local chromel–alumel

TABLE 1

Quantities Used in the Preparation of Supported Samples

	Materials used			Catalyst properties	
Sample	Silica (g)	Metal nitrate (mol)	$(NH_4)_2HPO_4$ (mol)	Phosphide loading (wt% M_xP)	Metal loading (mol% M)
Fe_2P/SiO_2	20	0.0462	0.0231	14	11
CoP/SiO_2	20	0.0231	0.0231	9.4	6.2
Ni_2P/SiO_2	20	0.0231	0.0231	9.4	6.1

thermocouple placed in a thermowell near the center of the reactor bed. The H_2 flow rate was set at 1000 μmol s^{-1} (1500 cm^3 min^{-1}) per g of sample. A portion of the exit gas flow was sampled through a leak valve into a mass spectrometer (Ametek/Dycor Model MA 100) and the masses 2(H_2), 4(He), 18(H_2O), 28(N_2), 32(O_2), 34(PH_3), 15(NH), 44(CO_2), 31(P), and 62(P_2) were monitored during the experiment, and these were recorded together with the temperature by an online computer. At the end of the temperature program, the sample was cooled in helium to room temperature and was passivated in a 0.5% O_2/He flow for 2 h.

Phosphide samples supported on a silica support were prepared by modifying the two-step procedure used in the synthesis of the unsupported samples. Aqueous phosphate solutions were obtained as before and were used to impregnate silica by the incipient wetness impregnation method. The quantities used for the three supported samples are listed in Table 1. Prior to use, the silica was dried at 393 K for 3 h and calcined at 773 K for 6 h and was found to have an incipient wetness point of 2.2 cm^3 g^{-1}. After impregnation, the powders were dried at 393 K for 3 h and calcined at 773 K for 6 h. The calcined samples were ground with a mortar and pestle, pelletized with a press (Carver, Model C), and sieved to 16/20 mesh size. The TPR process was similar to that used for the bulk samples using the same heating rate, $\beta = 0.0167$ K s^{-1} (1 K min^{-1}).

Characterization

The synthesized materials were characterized by CO chemisorption, N_2 physisorption, and X-ray diffraction (XRD) measurements. Irreversible CO uptake measurements were used to titrate the surface metal atoms and to provide an estimate of the number of active sites on the catalysts. Uptakes were obtained after passivated samples were rereduced and are denoted *ex situ* in this paper. Usually, 0.2 g of sample was loaded into a quartz reactor and treated in H_2 at 723 K for 2 h. After cooling to room temperature in He, pulses of CO in a He carrier flowing at 27 μmol s^{-1} (40 cm^3 NTP min^{-1}) were injected through a sampling valve and the 28 (CO) signal was monitored with a mass spectrometer. Uptakes of CO were also measured for the spent samples. The procedures were the same as those used for the fresh samples. Prior to the measurement, the spent samples removed from the hydrotreating reactors were washed in hexane and dried.

BET surface area measurements were carried out right after the CO uptake determinations, using a similar technique. Adsorption at liquid nitrogen temperature was performed using a 30% N_2/He stream, and the desorption area obtained after rapid heating was compared to the area of a calibrated volume (35.4 μmol). The surface area was calculated from the one-point BET equation, which is reasonable for nonmicroporous materials such as those used here. X-ray diffraction (XRD) patterns of the samples were determined with a Scintag XDS-2000 powder diffractometer operated at 45 kV and 40 mA, using Cu $K\alpha$ monochromatized radiation ($\lambda = 0.154178$ nm). The crystallite size of the supported sample was calculated using the Scherrer equation, $D_c = K\lambda/\beta\cos(\theta)$, where K is a constant taken as 0.9, λ is the wavelength of the X-ray radiation, β is the width of the peak at half-maximum, corrected for instrumental broadening (0.1°), and 2θ is the Bragg angle (34–36). The near-surface composition of the nickel samples was obtained by X-ray photoelectron spectroscopy (XPS) (Perkin–Elmer, Model 5300 with a Mg source) operated at 15 kV and 30 mA. The 285.0-eV binding energy peak of adventious carbon was used as reference. In the case of the spent catalysts, samples were removed from the reactor, washed in hexane, heated in H_2 to 673 K, and then passivated. Since the samples were exposed to the atmosphere and not sputtered, contamination by carbon from the atmosphere was present.

Reactivity Studies

Hydrotreating activities of the samples were obtained in a three-phase trickle-bed reactor for hydrodenitrogenation (HDN) and hydrodesulfurization (HDS) with a model petroleum liquid containing 2000 ppm nitrogen (quinoline), 3000 ppm sulfur (dibenzothiophene), 500 ppm oxygen (benzofuran), 20 wt% aromatics (tetralin), and balance aliphatics (tetradecane). The operating conditions were close to industrial conditions, 3.1 MPa and 643 K, with a liquid flow rate of 5 cm^3/h and a hydrogen flow rate of 100 μmol s^{-1}(150 cm^3 min^{-1}) corresponding to a gas–liquid ratio of 9800 SCF H_2/barrel. The detailed description of the testing system is reported elsewhere (37). Quantities of catalysts loaded in the reactor correspond to the same amount of *ex situ* CO uptake (35 μmol). Prior to reactivity measurements, the catalyst samples were pretreated in exactly the same manner as before the *ex situ* CO uptake determinations. Hydrotreating samples were collected every 2 or 3 h in sealed septum vials and were analyzed off-line with a gas chromatograph (Hewlett Packard, 5890A) equipped with a 0.32 mm i.d. × 50 m fused silica capillary column (CPSIL-5CB, Chrompack, Inc.) and a flame ionization detector.

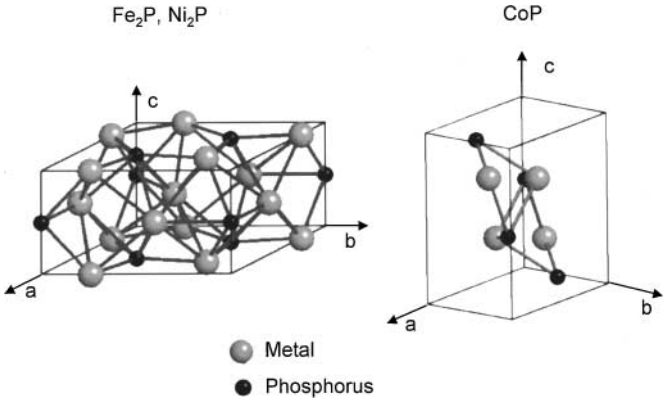

FIG. 1. Crystal structures of Fe_2P, CoP, and Ni_2P.

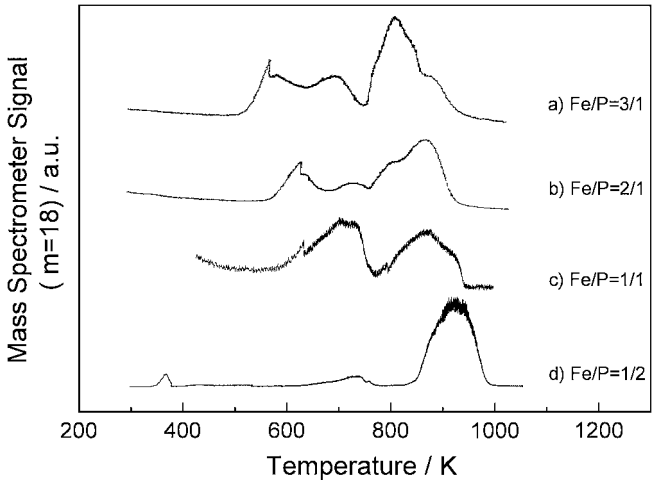

FIG. 2. Temperature-programmed reduction of bulk iron phosphates at $\beta = 1$ K/min (0.01667 K s^{-1}) (Fe-to-P ratios used in the preparation are indicated).

RESULTS AND DISCUSSION

Properties and Preparation of Bulk Phosphides

The crystal structures of the Fe, Co, and Ni phosphides are shown in Fig. 1 and their lattice parameters are summarized in Table 2. Both Fe_2P (38) and Ni_2P (39) adopt the same hexagonal structure (space group: $P_{\bar{6}2m}$), while CoP (40) takes on an orthorhombic structure (space group: P_{nma}). The crystal structures (Fig. 1) and lattice parameters can be used to calculate the bulk density (ρ) and the surface metal atom density ($\bar{n}$) of the solids (Table 2). For the Fe_2P and Ni_2P samples there are two, three, and two atoms on the *ac*, *ab*, and *bc* unit cell faces, respectively. For CoP, every unit cell face has two atoms.

The investigation of the phosphide materials in this study was begun by a study of the synthesis of bulk materials of various metal-to-phosphorus ratios (M/P) by the temperature-programmed method. This was carried out to prepare suitable references for the supported materials, and to evaluate the conditions of preparation needed when a support was employed.

The synthesis of the bulk phosphides involved two stages, preparation of phosphate precursors and reduction of the precursors in a temperature-programmed manner. The results for iron are discussed first. The precursors prepared in the first stage had different Fe/P ratios, set at the time of preparation by adjusting the mole ratio of the constituents. The precursors were formed by the thermal decomposition of mixtures of the metal nitrate and ammonium phosphate in air. Because the nitrate and ammonium ions are unstable at high temperature, it was expected that the mixture would decompose to a metal phosphate or metal oxide–phosphate. At high metal ratios some metal oxide was also likely. X-ray diffraction patterns of the precursors showed that they were amorphous.

Temperature-programmed reduction (TPR) of the precursors was carried out in the second stage (Fig. 2). Only the results for mass 18(H_2O) are shown, as the other monitored masses were featureless or provided little additional information. The TPR traces show two systematic trends for the samples with different Fe/P ratios. First, for higher Fe contents (Figs. 2a–2c), the TPR traces show more peaks and a more complicated overall reduction pattern. Second, for higher Fe contents, all the reduction peaks including the initial and final features are shifted to lower temperatures. These trends are reasonable. For higher Fe contents, the precursor is probably a mixture of iron oxide, iron phosphate, and possibly other components, and their separate reduction results in different peaks. Also for these higher Fe contents, the proportion of iron oxide should increase, and since this oxide is easily reducible, its TPR peaks appear at lower temperatures. In fact, it is likely that some metallic

TABLE 2

Surface Metal Density and Bulk Density of Fe_2P, CoP, and Ni_2P

Sample	Lattice parameter (nm)			Surface metal density (10^{15} atoms cm^{-2})				Compound density (ρ) (g cm^{-3})
	a	*b*	*c*	*ab* plane	*bc* plane	*ac* plane	Average ($\bar{n}$)	
Fe_2P	0.5867	0.5867	0.3458	1.01	0.986	0.986	0.994	6.67
CoP	0.5077	0.3281	0.5587	1.20	1.09	0.706	0.999	6.20
Ni_2P	0.5859	0.5859	0.3382	1.01	1.01	1.01	1.01	7.09

Fe is formed and that it assists in the reduction of the other components. For low Fe contents (Fig. 2d), there is no iron oxide and reaction occurs at the intrinsic reduction temperature of the main phosphate phase (~920 K). Because this temperature is high, even if a mixture of components other than phosphates existed, individual reduction steps cannot be resolved and the whole process appears to occur in one stage.

Analysis of the products of TPR was carried out by XRD (Fig. 3). The diffraction patterns all show a high background because of fluorescence by the iron. However, the presence of distinct iron phosphides can be seen easily. For the samples with Fe/P ratios of 3/1 and 2/1, the XRD results show the expected phases of Fe_3P (Fig. 2a) and Fe_2P (Fig. 3b). Comparison is made with standards from the powder diffraction file (PDF) (41), as indicated in the figure. For the sample with Fe/P ratio of 1/1, the obtained phase was still Fe_2P (Fig. 3c), and there was a deficiency in phosphorus. Similarly, for the sample with an Fe/P ratio of 1/2, the observed phase was FeP. Thus, although the preparations were carried out with stoichiometric quantities of metal and phosphorus, the final products tended to be metal-rich.

There are probably several processes which contributed to the loss of phosphorus in these samples. Some of the loss may have occurred during the TPR process, as traces of PH_3 were detected in the mass spectrometer signal and some volatile products were observed to condense at the exit of the reactor. Some of the loss probably also occurred in the calcination step at 773 K to form the phosphate precursor. A small amount of a white solid was found to have sublimed onto the lid of the ceramic calcination vessel. This was likely to be P_2O_5, with a melting point of 563 K and a sublimation temperature of 787 K. The loss of P was observed in all

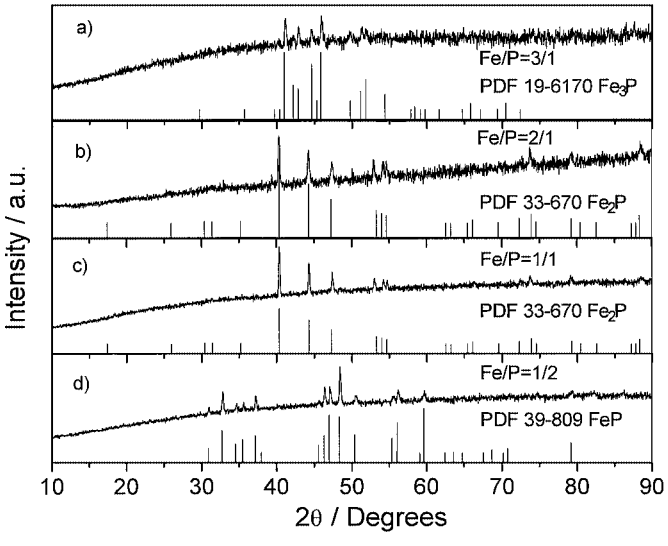

FIG. 3. X-ray diffraction patterns of iron phosphides (PDF file references are also included).

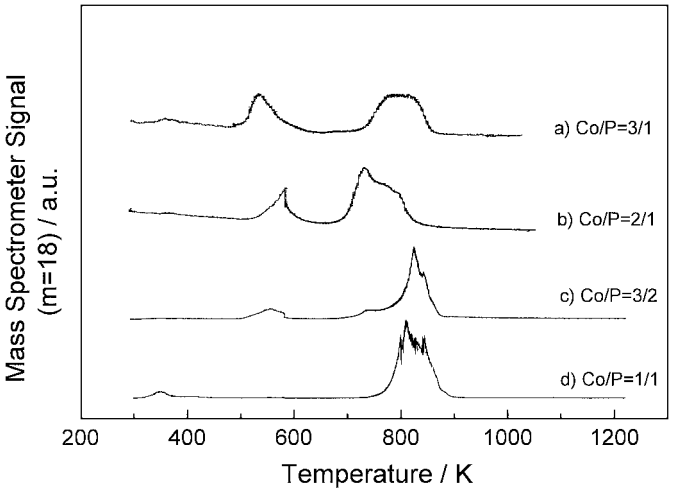

FIG. 4. Temperature-programmed reduction of bulk cobalt phosphates at $\beta = 1$ K/min (0.01667 K s^{-1}) (Co-to-P ratios used in the preparation are indicated).

samples with high P levels. There is also a possibility that some extra phosphorus in amorphous form remained mixed in the samples, and that the observed phases were simply the stable ones under the preparation conditions.

The trends in the TPR results for the cobalt samples (Fig. 4) are similar to those of the iron samples. The reaction traces consist of two main features, a low-temperature peak and a more complicated high-temperature signal. (The sample with Co/P = 1/1 has a small feature at ~350 K, probably due to dehydration). The low-temperature peak appears between 500 and 600 K and is more intense for higher Co contents (Figs. 4a–4c). It also shifts to lower temperature with increasing Co content. This behavior is consistent with the reduction of a cobalt oxide species. The higher temperature signal appears between 700 and 900 K and probably corresponds to the reduction of cobalt phosphate, which is expected to be more difficult to reduce. It is the main feature for the Co/P = 1/1 sample (Fig. 4d). The XRD patterns of the reduced cobalt samples (Fig. 5) show that Co_2P was obtained from the samples with Co/P ratios of 3/1, 2/1, and 3/2 (Figs. 5a–5c), and CoP was obtained as expected from the sample with a Co/P ratio of 1/1 (Fig. 5d). It appears that Co_2P is a particularly stable phase at these conditions.

The same trends in the TPR traces were also observed with the nickel samples (Fig. 6). The reduction features were a composite of different peaks, occurring at a low-temperature range of 500–700 K, and at a high-temperature range of 700–850 K. These various features are attributed again to the reduction of different compounds, likely nickel oxides and nickel oxide phosphate at the low temperatures and nickel phosphate at the high temperatures. As expected, Ni_3P was observed in the sample with a Ni/P ratio of 3/1 (Fig. 7a). But for the Ni/P ratios of 2/1, 3/2, and 1/1 (Figs. 7b–7d), the phase obtained was Ni_2P. Probably, this is

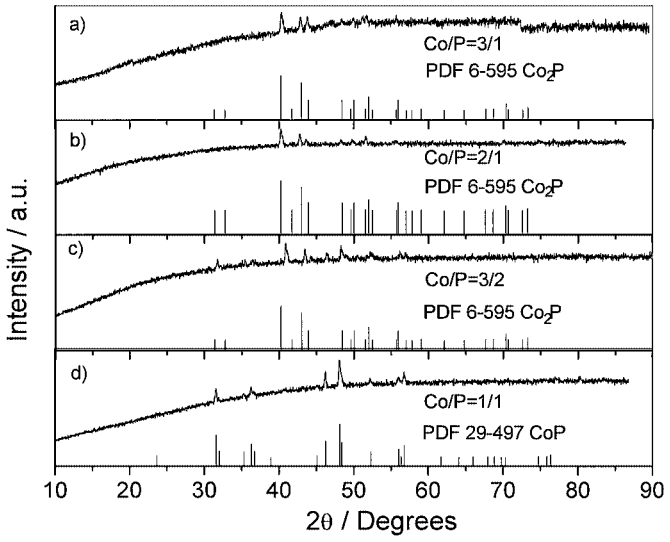

FIG. 5. X-ray diffraction patterns of reduced cobalt phosphates (PDF file references are also included).

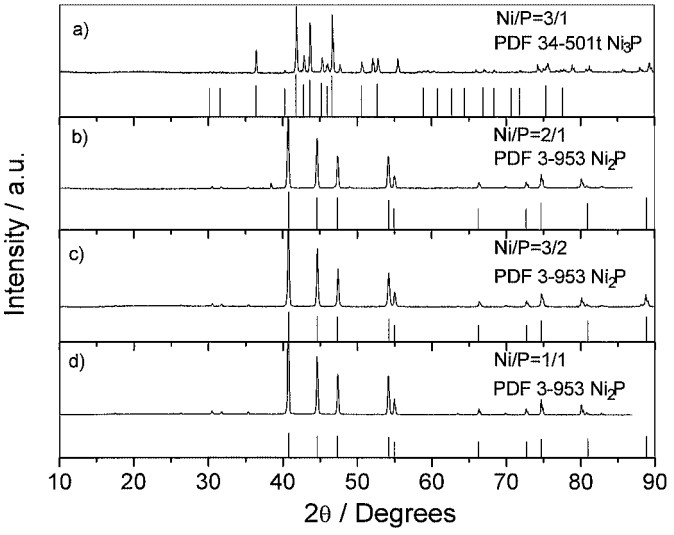

FIG. 7. X-ray diffraction patterns of reduced nickel phosphates (PDF file references are also included).

the stable phase at the conditions of the preparation, since not all the phosphorus in the precursor phosphate mixtures is likely to have sublimed. Different from the other samples, the TPR trace of the sample with the Ni/P ratio of 1/1 did show some P and PH_3 during the reduction process. This accounts for the loss of P in this sample.

To summarize these TPR and XRD results, the reduction of phosphate precursors occurs readily in the Fe, Co, and Ni systems, with maximum temperatures of about 900 K. A number of bulk phosphide compounds can be produced, depending on the stoichiometric proportions of M/P used, but the Fe_2P, CoP, and Ni_2P products are the preferred phases under the experimental conditions used in this study.

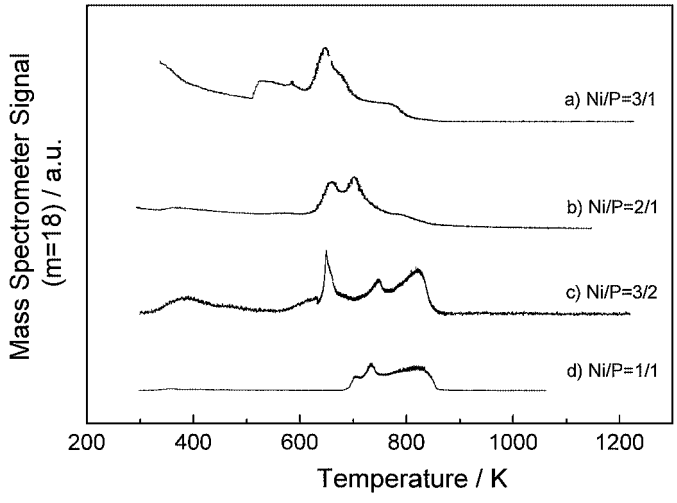

FIG. 6. Temperature-programmed reduction of bulk nickel phosphates at $\beta = 1$ K/min (0.01667 K s^{-1}) (Ni-to-P ratios used in the preparation are indicated).

Properties and Preparation of Supported Phosphides

In order to study the catalytic properties of the Fe, Co, and Ni samples high-surface-area materials were desired, and therefore, the phosphides were prepared in supported form using silica as the carrier. The preparation involved the same steps used in the synthesis of the bulk compounds. First, phosphates were prepared on the support and then were reduced by TPR. The final temperatures for preparing hydrotreating catalysts were determined by noting the point where the intensity of the water signal returned to baseline in preliminary TPR test measurements on small samples. The final temperature for supported iron, cobalt, and nickel samples were 1000, 900, and 850 K, respectively (Fig. 8). Silica was selected as the carrier because in dehydrated form it has few acid and base sites and is likely to

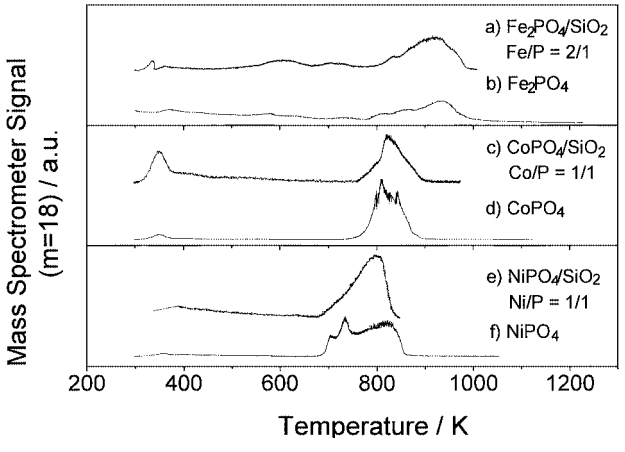

FIG. 8. TPR comparison of supported and unsupported catalysts at $\beta = 1$ K/min (0.01667 K s^{-1}).

TABLE 3

Characterization Results of Samples

Samples	BET surface area (S_g/m^2 g^{-1})	CO uptake (μmol g^{-1})	D_p (nm)	D_c (nm)	Metal site concentration (μmol g^{-1})
Fe_2P	2.7	3	330	38	45
Fresh Fe_2P/silica	97	16		23	90
Spent Fe_2P/silica	83	0		23	90
CoP	3.1	3	310	40	51
Fresh CoP/silica	87	16		21	72
Spent CoP/silica	90	4		21	72
Ni_2P	3.3	4	260	36	55
Fresh Ni_2P/silica	98	15		20	67
Spent Ni_2P/silica	100	13		20	67

offer minimal support interaction to affect the properties of the phosphides. Thus, the intrinsic activity of the phosphides could be determined.

Comparison of the TPR results obtained for the bulk samples and the corresponding supported samples (Fig. 8) provides strong evidence that the transformation of the phosphates to phosphides proceeded in the same manner for both bulk and supported samples. Aside from a slightly more pronounced low-temperature dehydration feature for the supported samples, the TPR traces for the samples of iron and cobalt were very similar to those of the unsupported forms. The reduction trace of the supported nickel sample was somewhat simpler than that of the bulk sample, but occurred at essentially the same temperature range.

The characterization results for the bulk and supported samples are reported in Table 3. The specific surface areas (S_g) of the bulk materials were low, approximately 3 m^2 g^{-1}, while those of the supported materials were close to that of the support (90 m^2 g^{-1}). The experimental CO uptakes of the samples are reported in the third column of Table 3. They were low for the bulk materials but increased for the supported samples.

The particle diameter of the bulk materials was calculated by the equation $D_P = 6/\rho S_g$ using their surface area and the bulk density (Table 2). The particle sizes for the bulk Fe_2P, CoP, and Ni_2P samples were similar, about 260–330 nm (Table 3). The crystallite sizes (D_c) were obtained from the Scherrer equation presented in the experimental section. The crystallite sizes for the bulk phosphides were again similar, about 36–40 nm. For all the bulk samples, $D_p > D_c$, and this could be due to strain and disorder in the crystallites or crystallite agglomeration. The latter is probably the larger contributor, as no support was used to stabilize the samples.

The last column in Table 3 reports the theoretical metal site concentration assuming that the samples were composed of uniform spherical particles. It was calculated from the equation

$$\text{Metal site concentration} = S_g \cdot \bar{n} \cdot f,$$

where S_g is specific surface area, $\bar{n}$ is the surface metal atom density, and f is the fractional weight loading (e.g., grams of Fe_2P/gram of catalyst) of the sample (Table 1). For the bulk samples the actual S_g was employed, while for the supported samples it was calculated from the crystallite size using the equation $S_g = 6/\rho D_c$. The last factor, f, accounts for the loading of the active phase on the supported samples.

In all cases the experimental CO uptake was considerably smaller (average 6.6% for the bulk samples; average 20.5% for the fresh supported samples) than the theoretically expected metal site concentration (Table 3) for a clean surface. This indicates that possibly the surface is blocked by some species that prevents adsorption, such as phosphorus or unreduced oxygen. In the case of transition metal carbides it is found that oxygen uptakes are considerably higher than CO uptakes (42, 43), and this suggests that oxygen should be tried as a chemisorption probe.

The effect of the heating rate on the peak temperature (T_p) associated with the reduction of supported catalysts (Fig. 9) was briefly examined in this work. The peak positions for water formation shifted to a temperature about 40–60 K higher as the heating rate (β) was increased from 0.0167 (1 K min^{-1}) to 0.0833 K s^{-1} (5 K min^{-1}). According to temperature-programmed reaction theory (44), the peak temperature (T_p) is related to the heating rate (β) and the apparent activation energy (E_a) (Table 4) by the Redhead equation ($2 \ln T_p - \ln \beta = E_a/RT_p + \text{Constant}$) (44). The activation energies found for Fe_2P/silica, CoP/silica, and Ni_2P/silica were 200, 220, and 150 kJ mol^{-1}, respectively. The results here are comparable with the activation energy

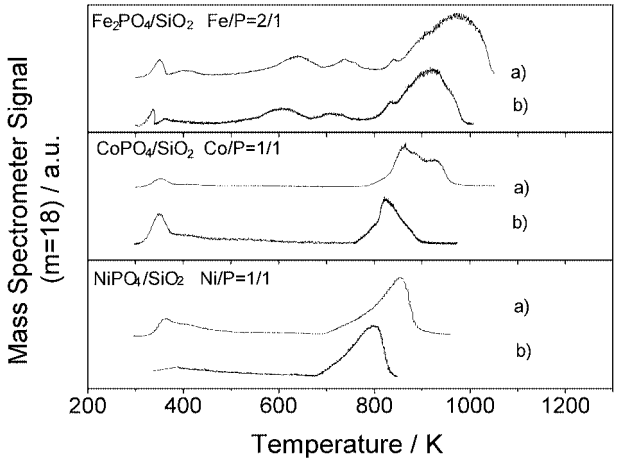

FIG. 9. TPR profiles of supported catalysts at different heating rates (β). (a) $\beta = 5$ K/min (0.08333 K s^{-1}); (b) $\beta = 1$ K/min (0.01667 K s^{-1}).

TABLE 4

Apparent Activation Energy (E_a) of Synthesis of the Supported Catalysts

Samples	E_a (kJ mol^{-1})
Fresh 14 wt% Fe_2P/silica	200
Fresh 9.4 wt% CoP/silica	220
Fresh 9.4 wt% Ni_2P/silica	150

of oxygen diffusion in the corresponding metal oxides, FeO, CoO, and NiO, which are 126, 144, and 166 kJ mol^{-1}, respectively, with preexponential factors of 1.4×10^{-2}, 2.15×10^{-3}, and 2×10^{-4} cm^2 s^{-1} (45). The correspondence is reasonable, as many solid state transformations are governed by diffusion processes (46).

Catalytic Activity in Hydroprocessing

Figures 10 and 11 present the HDS and HDN activities for the reactions of dibenzothiophene and quinoline, respectively. All three samples have high initial activities for HDS and HDN. However, except for the nickel sample in HDS, all catalysts undergo deactivation. The Fe_2P/SiO_2 lost all HDS and HDN activity by 60 h, while the CoP/SiO_2 appeared to reach a baseline of about 32% HDS and 31% HDN at around 100 h. Only the Ni_2P/SiO_2 had good, stable activity in HDS. The HDS sequence for the three samples was $Ni_2P/SiO_2 > CoP/SiO_2 > Fe_2P/SiO_2$, while the HDN sequence was $CoP/SiO_2 > Ni_2P/SiO_2 > Fe_2P/SiO_2$. Compared with a commercial Ni–Mo–S/γ-Al_2O_3 catalyst at the same conditions (24), Ni_2P/SiO_2 had a higher HDS activity, with 90 versus 76% conversion, but a lower HDN activity, with 14 versus 38% conversion. The measurements were made on the basis of equal chemisorption sites loaded in the reactor (35 μmol for the phosphides, 33 μmol for the sulfide). For the phosphides CO at room temperature was used for the chemisorption and for the sulfide O_2 at dry ice/acetone temperature was used. It may be that the CO chemisorption underestimates sites on the phosphide, so the conversions should be taken just as an approximation of intrinsic activity.

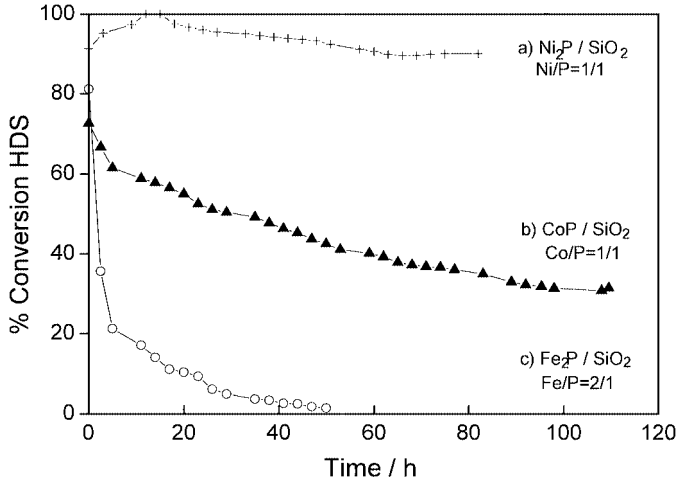

FIG. 10. Hydrodesulfurization performance of supported catalysts. (Basis: 35 μmol of chemisorption sites).

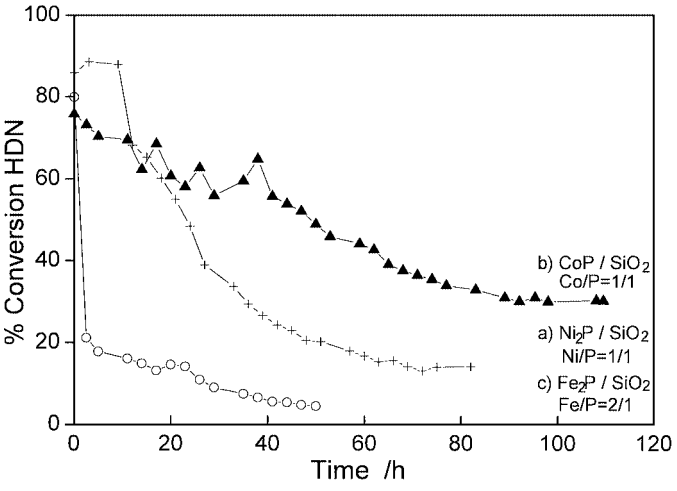

FIG. 11. Hydrodenitrogenation performance of supported catalysts. (Basis: 35 μmol of chemisorption sites).

A listing of conversions and selectivities for all the reactions is provided in Table 5. For dibenzothiophene the only product observed was biphenyl. However, for quinoline a number of species were obtained, and these were categorized as HDN products and hydrogenation (HYD) products. For benzofuran, again only one product was obtained, ethylbenzene. The amount of benzofuran used was small (500 ppm) and the reaction is facile so is unlikely to interfere with the HDS and HDN reactions, as known from other studies with carbides, nitrides, and sulfides (47, 48). In the case of tetralin, at the reaction conditions the major species obtained was the dehydrogenation product naphthalene, although small amounts of *cis*- and *trans*-decalin were also observed.

Turnover rates and areal rates measured at the baseline levels are listed in Table 6. The basis of comparison is now 70 μmol of sites, to make the numbers directly comparable to others published elsewhere (49). The procedure for conversion assumes a first-order reaction and is given in the footnotes of the table. The turnover rates are based on the experimentally determined CO uptakes on the fresh catalysts, while the areal rates are based on the calculated surface area of the phosphide crystallites using $S_g = 6/\rho D_c$ and the weight loading factor f. The Fe_2P catalyst deactivated completely and its rate is reported as zero. The CoP/SiO_2 had areal rates of 1.4×10^{15} mol m^{-2} s^{-1} in HDS and 2.1×10^{15} mol m^{-2} s^{-1} in HDN, while the Ni_2P/SiO_2 had rates of 3.4×10^{15} mol m^{-2} s^{-1} in HDS and 1.4×10^{15} mol

TABLE 5

Product Distribution in Hydroprocessing[a]

Reactants	Conversion (%)			Selectivity (%)		
	Type	Ni_2P/SiO_2	CoP/SiO_2	Product	Ni_2P/SiO_2	CoP/SiO_2
Dibenzothiophene	HDS	90	32	Biphenyl	100	100
Quinoline	HDN	14	31	Propylcyclohexane	4	16
	HYD	44	49	Propylbenzene	9	9
				5,6,7,8-Tetrahydroquinoline	33	30
				Orthopropylaniline	31	23
				1,2,3,4-Tetrahydroquinoline	24	22
Benzofuran	HDO	35	11	Ethylbenzene	100	100
Tetralin	deHYD	31	6.5	Naphthalene	98.2	91.5
	HYD	0.6	0.6	*trans*-Decalin	0.6	3.6
				cis-Decalin	1.2	4.9

[a] Catalyst loaded was equivalent to 35 μmol of CO uptake sites.

TABLE 6

Rates of HDS and HDN of the Supported Catalysts

Sample	Turnover rate[a] (10^{-3} s^{-1})		Areal rate[b] (10^{15} mol m^{-2} s^{-1})		Specific rate[c] (10^{8} mol g^{-1} s^{-1})		Volumetric rate[d] (10^{9} mol cm^{-3} s^{-1})	
	HDS	HDN	HDS	HDN	HDS	HDN	HDS	HDN
Fe_2P/SiO_2	0	0	0	0	0	0	0	0
CoP/SiO_2	0.81	1.2	1.4	2.1	1.3	1.9	4.8	7.0
Ni_2P/SiO_2	1.5	0.60	3.4	1.4	2.2	0.9	8.1	0.33

[a] Calculated from $r_t = QX/S$, where Q is the molar rate of reactant, X is the conversion, and S is the mole of sites loaded. The basis used was 70 μmol. Conversions were adjusted using the first-order formula $X_2 = 1-(1-X_1)^{S_2/S_1}$, where $S_2/S_1 = 70\ \mu\text{mol}/35\ \mu\text{mol} = 2$, and gave higher X than reported in Table 5 (CoP: HDS, 54%, HDN, 52%; Ni_2P: HDS, 99%, HDN, 26%).

[b] Calculated from $r_A = QXN_A/WS_g f$, where N_A is Avogadro's number, W is the weight of catalyst, S_g is the metal phosphide surface area, and f is the fractional loading of phosphide.

[c] Calculated from $r_S = r_t$(CO uptake).

[d] Calculated from $r_V = r_S\rho$, where ρ is the apparent density of the catalysts, ~0.37 g cm^{-3}.

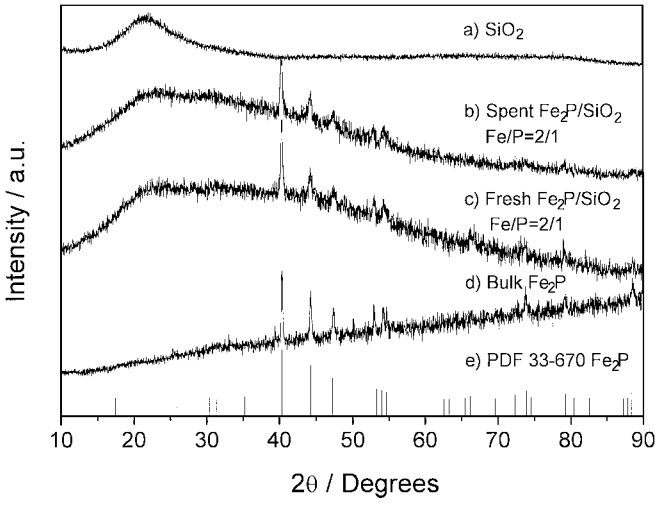

FIG. 12. X-ray diffraction patterns of iron phosphides and references. (a) Blank sample, SiO_2; (b) spent sample, Fe_2P/SiO_2; (c) fresh sample, Fe_2P/SiO_2; (d) bulk sample, Fe_2P; and (e) PDF 33-670 Fe_2P (Ref. 41).

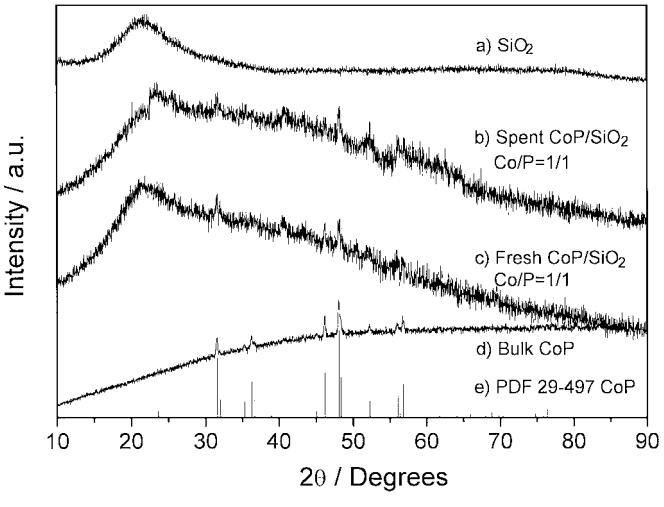

FIG. 13. X-ray diffraction patterns of cobalt phosphides and references. (a) Blank sample, SiO_2; (b) spent sample, CoP/SiO_2; (c) fresh sample, CoP/SiO_2; (d) bulk sample, CoP; and (e) PDF 29-497 CoP (Ref. 41).

m^{-2} s^{-1} in HDN. In a recent study of the HDN on unsupported samples Stinner *et al.* report areal rates of 4.8×10^{16} mol m^{-2} s^{-1} on Co_2P and 5.8×10^{16} mol m^{-2} s^{-1} on Ni_2P (26). The higher HDN rates on those samples can be attributed to several factors. First, Stinner *et al.* studied only HDN and employed a more reactive substrate (*o*-propylaniline rather than quinoline), which probably led to higher rates. They also carried out their tests without using sulfur compounds in the feed. Sulfur compounds can lead to competitive adsorption and lower rates. Finally, Stinner *et al.* used low-surface-area (1–3 m^2 g^{-1}) unsupported materials in a low-conversion regime, which would tend to result in higher rates. Nevertheless, despite the differences in experimental conditions the rates are of similar orders of magnitude.

The XRD patterns of the silica support, fresh phosphide samples, spent samples, and PDF references are compared in Figs. 12–14. These results show that silica did not influence the phases of the phosphides formed, which were the same as those obtained in the bulk materials Fe_2P, CoP, and Ni_2P. The XRD patterns for the spent iron and cobalt samples were unchanged from the corresponding fresh samples, which shows that the Fe_2P phase (Fig. 12) and CoP phase (Fig. 13) are stable during the hydrotreating reaction. For the spent nickel sample, one more peak was observed (Fig. 14). Comparing this pattern with those of other nickel phosphide compounds, it was found that the peak (*) matched one due to $Ni_{12}P_5$. This indicated that possibly a part of the Ni_2P phase transformed to a $Ni_{12}P_5$-like phase during hydrotreating. XPS measurement for this sample (Table 7) showed a P/Ni ratio close to 1 for the fresh sample, which decreased to 0.77 for the spent catalyst. This decrease may be related to the drop in HDN activity for this sample. The XPS analysis surprisingly also indicated a lack of S or N on the spent sample. The measurements were repeated on samples treated in He (just to remove volatile compounds), but the results were the same. This is likely due to lack of sensitivity by XPS at the levels expected for surface sulfur species in these supported samples. Already the signals for Ni and P were very low.

The results of posthydrotreating characterization are also presented in Table 3. For the iron sample, the CO uptake decreased to zero after the hydrotreating. The loss of the CO uptake is likely associated with the dramatic deactivation of the iron sample (Figs. 10c and 11c). As to the spent cobalt sample, the CO uptake also decreased substantially, but not to zero, as in the case of the iron sample. This was in line with the less complete deactivation of the catalyst. In the case of nickel, again a decrease in CO uptake was observed, but the decrease was much smaller than those of the iron and cobalt samples. Overall, the trend appears to indicate that the decrease in catalytic performance is related to the loss of active sites.

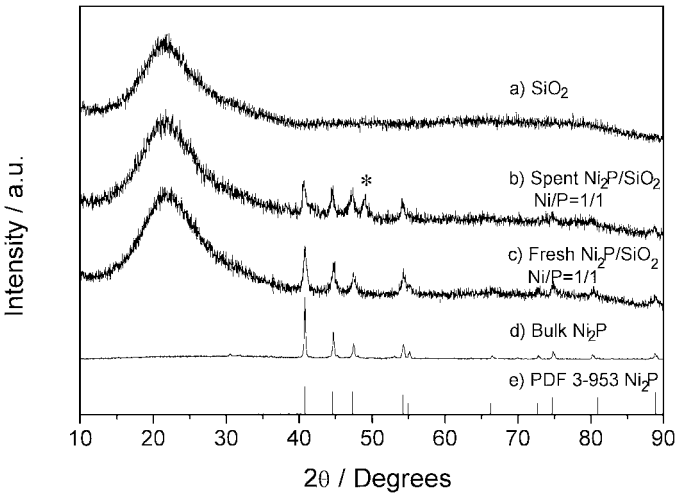

FIG. 14. X-ray diffraction patterns of nickel phosphides and references (a) Blank sample-SiO_2; (b) spent sample Ni_2P/SiO_2; (c) fresh sample Ni_2P/SiO_2; (d) bulk sample Ni_2P; and (e) PDF 3-953 Ni_2P (Ref. 41).

The reduction in the number of active sites is apparently caused by sulfidation of the catalysts. This is currently being investigated by extended X-ray absorption spectroscopy (EXAFS) of the fresh and spent samples (49). The results indicate that the catalysts are phase pure and sulfidation is restricted to the surface of the phosphide crystallites, as X-ray diffraction analysis shows that the phosphide phase is retained. The surface sulfidation process appears to be more pronounced in iron and cobalt phosphide, which show considerable deactivation in HDS and HDN. The nickel phosphide appears to be more tolerant to sulfur and thus retains high HDS activity. This is entirely reproducible. Its HDN activity is lowered, probably because the latter reaction is structure sensitive (49), and the site requirements for nitrogen removal are disrupted.

TABLE 7

XPS Results for Supported Nickel Samples

Fresh 9.4 wt% Ni_2P/silica	Element	C 1s	O 1s	N 1s	S 2p	P 2p	Ni 2p	Si 2p
	Concentration (%)	16.73	55.42	0	0	0.80	0.83	26.22
Spent 9.4 wt% Ni_2P/silica	Element	C 1s	O 1s	N 1s	S 2p	P 2p	Ni 2p	Si 2p
	Concentration (%)	19.24	53.16	0	0	0.36	0.47	26.77

CONCLUSIONS

Pure Fe_2P, CoP, and Ni_2P phases were successfully synthesized by means of temperature-programmed reduction of the corresponding phosphates. The silica-supported forms of these samples were also successfully prepared, with retention of the active phase and increased CO uptake and BET surface area. It was found that Fe_2P/SiO_2 had good initial activity for HDS of dibenzothiophene and HDN of quinoline, but that this activity fell to zero in about 60 h. The CoP/SiO_2 catalyst also deactivated but appeared to reach a stable baseline of 32% HDS and 31% HDN conversion. Only the Ni_2P/SiO_2 had a stable and high conversion in HDS of 90%, although its HDN was low at 14%. The deactivation in all cases was associated with a decrease in the number of surface metal sites as titrated by the chemisorption of CO. For the most promising catalyst, Ni_2P/SiO_2, HDS was higher than that of a commercial catalyst, Ni–Mo–S/γ-Al_2O_3, based on equal sites loaded in the reactor, as measured by CO uptake for the phosphide and low-temperature O_2 chemisorption for the sulfide. The development and improvement of this group of phosphides in the hydroprocessing field is a promising area of research.

ACKNOWLEDGMENTS

The authors are indebted to the Department of Energy (DOE) Office of Basic Energy Science, Grant DE-FG02-96ER14669, for financial support and to the NEDO International Joint Research Grant Program.

REFERENCES

1. U.S. Environmental Protection Agency, Press Release, May 1, 1999; December 21, 2000.
2. "Federal Register," Vol. 65, No. 28. U.S. Govt. Printing Office, Washington, DC, 2000.
3. O'Connor, P., and Mayo, S., *ACS Prep. Div. Fuel Chem.* **46**, 381 (2001).
4. Topsøe, H., Clausen, B. S., and Massoth, F. E., *in* "Hydrotreating Catalysis, Science and Technology" (J. R. Anderson and M. Boudart, Eds.), Vol. 11. Springer-Verlag, Berlin/Heidelberg/New York, 1991.
5. Aronsson, B., Lundström, T., and Rundqvist, S., "Borides, Silicides and Phosphides." Wiley, New York, 1965.
6. Boudart, M., Cusumano, J. A., and Levy, R. B., "New Catalytic Materials for the Liquefaction of Coal, Research Project 415, Final Report," p. 184. Catalytica Associates, Inc., 5 Palo Alto Square, Palo Alto, CA, 1975.
7. Damyanova, S., Spojakina, A., and Vit, Z., *Collect. Czech. Chem. Commun.* **57**, 1033 (1992).
8. Ozkan, U. S., Zhang, L. P., Ni, S. Y., and Moctezuma, E., *J. Catal.* **148**, 181 (1994).
9. Gulková, D., and Zdražil, M., *Collect. Czech. Chem. Commun.* **64**, 735 (1999).
10. Poulet, O., Hubaut, R., Kasztelan, S., and Grimblot, J., *Bull. Soc. Chim. Belg. Eur. Sec.* **100** (11–12), 857 (1991).
11. Fitz, C. W., Jr., and Rase, H. F., *Ind. Eng. Chem. Prod. Res. Dev.* **22**, 40 (1983).
12. Lewis, J. M., Kydd, R. A., Boorman, P. M., and Van Rhyn, P. H., *Appl. Catal. A* **84**, 103 (1992).
13. Jian, M., Rico Cerda, J. L., and Prins, R., *in* "Vth Workshop on Hydrotreating Catalysis, European Section, Lille-Villeneuve d'Ascq," p. 225. 1995.
14. Jian, M., and Prins, R., *Catal. Lett.* **35**, 193 (1995).
15. Atasanova, P., Tabakova, T., Vladov, Ch., Halachov, T., and Lopez Agudo, A., *Appl. Catal. A* **161**, 105 (1997).
16. Mangnus, P. J., van Veen, J. A. R., Eijsbouts, S., De Beer, V. H. J., and Moulijn, J. A., *Appl. Catal.* **61**, 99 (1990).
17. Iwamoto, R., and Grimblot, J., *Adv. Catal.* **44**, 417 (1999).
18. Chadwick, D., Aitchison, D. W., Badilla-Ohlbaum, R., and Josefsson, L., *Stud. Surf. Sci. Catal.* **16**, 323 (1982).
19. Eijsbouts, S., van Gestel, J. N. M., van Veen, J. A. R., de Beer, V. H. J., and Prins, R., *J. Catal.* **131**, 412 (1991).
20. López Agudo, A., López Cordero, R., Palacios, J. M., and Fierro, J. L., *in* "Vth Workshop on Hydrotreating Catalysis, European Section, Lille-Villeneuve d'Ascq," p. 237. 1995.
21. Robinson, W. R. A. M., van Gestel, J. N. M., Korányi, T. I., Eijsbouts, S., van der Kraan, A. M., van Veen, J. A. R., and de Beer, V. H. J., *J. Catal.* **161**, 539 (1996).
22. Li, W., Dhandapani, B., and Oyama, S. T., *Chem. Lett.* 207 (1998).
23. Oyama, S. T., Clark, P., Teixeira da Silva, V. L. S., Lede, E. J., and Requejo, F. G., *J. Phys. Chem. B* **105**, 4961 (2001).
24. Clark, P., Li, W., and Oyama, S. T., *J. Catal.* **200**, 140 (2001).
25. Stinner, C., Prins, R., and Weber, Th., *J. Catal.* **191**, 438 (2000).
26. Stinner, C., Prins, R., and Weber, Th., *J. Catal.* **202**, 187 (2001).
27. Nozaki, F., Kitoh, T., and Sodesawa, T., *J. Catal.* **62**, 286 (1980).
28. Nozaki, F., and Tokumi, M., *J. Catal.* **79**, 207 (1983).
29. Nozaki, F., and Adachi, R., *J. Catal.* **40**, 166 (1975).
30. Wang, W., Qiao, M., Li, H., and Deng, J., *Appl. Catal. A* **166**, L243 (1998).
31. Robinson, W. R. A. M., van Gestel, J. N., Korányi, M., Eijsbouts, T. I. S., van der Kraan, A. M., van Veen, J. A. R., and de Beer, V. H. J., *J. Catal.* **161**, 539 (1996).
32. Lee, S.-P., and Chen, Y.-W., *J. Mol. Catal. A* **152**, 213 (2000).
33. Li, H., Wang, W., Li, H., and Deng, J.-F., *J. Catal.* **194**, 211 (2000).
34. Guinier, A., *in* "X-Ray Diffraction in Crystals, Imperfect Crystals, and Amorphous Bodies," p. 121. Freeman, San Francisco, 1963.
35. Warren, B. E., *in* "X-Ray Diffraction," p. 254. Addison-Wesley, Menlo Park, CA, 1969.
36. Cullity, B. D., *in* "Elements of X-Ray Diffraction," 2nd ed., p. 102. Addison-Wesley, Menlo Park, CA, 1978.
37. Ramanathan, S., and Oyama, S. T., *J. Phys. Chem.* **99**(44), 16365 (1995).
38. Carlsson, B., Gölin, M., and Rundqvist, S., *J. Sol. St. Chem.* **8**, 57 (1973).
39. Rundqvist, S., *Acta Chem. Scand.* **16**, 992 (1962).
40. Rundqvist, S., *Acta Chem. Scand.* **16**, 287 (1962).
41. "Powder Diffraction Data Files." JCPDS International Center for Diffraction Data, Swathmore, PA, 1992.
42. St. Clair, T. P., Dhandapani, B., and Oyama, S. T., *Catal. Lett.* **58**, 169 (1999).
43. St. Clair, T. P., Oyama, S. T., and Cox, D. F., *Surf. Sci.* **468**, 62 (2000).
44. Boudart, M., and Djéga-Mariadassou, G., *in* "Kinetics of Heterogeneous Catalytic Reactions, Physical Chemistry: Science and Engineering," p. 57. Princeton University Press, Princeton, NJ, 1984.
45. O'Keeffe, M., *in* "Diffusion in Oxide and Sulfides, Sintering and Related Phenomena, Proc. Intl. Conf." (G. C. Kuczynski, N. A. Hooton, and C. F. Gibbon, Eds.). Gordon and Breach, New York, 1967.
46. Bruke, J., "The Kinetics of Phase Transformations in Metals," Pergamon, Oxford, 1965.
47. Dhandapani, B., St. Clair, T., and Oyama, S. T., *Appl. Catal. A* **168**, 219 (1998).
48. Ramanathan, S., Yu, C. C., and Oyama, S. T., *J. Catal.* **173**, 10 (1998).
49. Wang, X., Lee, Y.-K., Oyama, S. T., Bando, K., and Requejo, F. G., submitted for publication.